Journal of Science: Advanced Materials and Devices 8 (2023) 100608

Contents lists available at ScienceDirect

Journal of Science: Advanced Materials and Devices

journal homepage: www.elsevier.com/locate/jsamd

Original Article

Control of magnetic vortex states in FeGa microdisks: Experiments and micromagnetics

Gajanan Pradhan [a, b, *], Alessandro Magni [a], Federica Celegato [a], Marco Coisson [a], Gabriele Barrera [a], Lenka Mikuličková [c], Jon Ander Arregi [d], Ladislav Čelko [d], Vojtěch Uhlíř [d], Paola Rizzi [b], Paola Tiberto [a]

[a] Advanced Materials and Life Science Divisions, Istituto Nazionale di Ricerca Metrologica (INRIM), Strada delle Cacce, 91, Turin, 10135, Italy
[b] Chemistry Department and NIS, University of Turin, Via Pietro Giuria, 7, Turin, 10125, Italy
[c] Thin Film Technological Service s.r.o., Novodvorska, 994-138, Prague, 14200, Czech Republic
[d] Central European Institute of Technology (CEITEC), Brno University of Technology, Purkynova, 123, Brno, 61200, Czech Republic

ARTICLE INFO

Article history:
Received 21 February 2023
Received in revised form
2 July 2023
Accepted 8 July 2023
Available online 14 July 2023

Keywords:
Magnetic vortex
Magneto-optic Kerr effect
Magnetic force microscope
Micromagnetic simulations

ABSTRACT

Magnetic vortices have been an interesting element in the past decades due to their flux-closure domain structures which can be stabilized at ground states in soft ferromagnetic microstructures. In this work, vortex states are shown to be nucleated and stabilized in $Fe_{80}Ga_{20}$ and $Fe_{70}Ga_{30}$ disks, which can be an upcoming candidate for applications in strain-induced electric field control of magnetic states owing to the high magnetostriction of the alloy. The magnetization reversal in the disks occurs by the formation of a vortex, double vortex or S-domain state. Micromagnetic simulations have been performed using the FeGa material parameters and the simulated magnetic states are in good agreement with the experimental results. The studies performed here can be essential for the use of FeGa alloy in low-power electronics.

1. Introduction

Magnetic vortex states have been studied quite extensively in the past two decades due to its potential to be used in memory applications and microwave oscillators [1–8]. These states have topologically stable spin configurations which are suitable to be formed in confined small-scale ferromagnetic structures like squares or disks [9]. The suitable materials for stabilizing a vortex are the ones with a soft magnetic behavior, where a good balance between exchange and dipolar energies exists. The stabilization of a single vortex state depends largely on the size of the magnetic element. An experimental phase diagram in the diameter and thickness of disks was studied by Cowburn et al. [10]. Single domain states are preferred for small disks below the vortex regime and multi domain states are stabilized for larger sizes. The vortices are defined by two fundamental quantities, i.e., the character of in-plane spin rotations (circularity, c) and the out-of-plane component (polarity, p). The clockwise (CW) and counter-clockwise (CCW) rotations correspond to $c = -1$ and $+1$, respectively. The polarization can point up ($p = +1$) or down ($p = -1$). The combination of c and p will result in four different states. The first report on lifting the degeneracy of these states was given by Im et al. where the authors demonstrated both experimentally and with micromagnetic simulations that the two groups, $cp = +1$ and $cp = -1$ can have different probabilities in formation [11]. This symmetry breaking is explained by the presence of intrinsic Dzyaloshinskii–Moriya interaction (DMI) having broken inversion symmetry or due to other surface related defects. The shape of a magnetic element like a rectangle or an ellipse can also favor different vortex states [12–15].

Magnetization reversal mechanisms have been studied in circular disks at micron and nano scale with various materials like NiFe [16–18], Co [19–21], FePd [22] etc. The disks stabilizing a vortex state at remanence have a typical hysteresis behavior. The nucleation occurs at a field value lower than the saturation field, termed as the nucleation field and the vortex gets annihilated before the saturation field intensity along the opposite direction. The spin direction along a vortex core was observed by Wachowiak et al. using spin-polarized scanning tunneling microscope (STM) and the change of out-of-plane and in-plane magnetization

* Corresponding author. Advanced Materials and Life Science Divisions, Istituto Nazionale di Ricerca Metrologica (INRiM), Torino, 10135, Italy.
E-mail addresses: gajananpradhan2@gmail.com, g.pradhan@inrim.it (G. Pradhan).

Peer review under responsibility of Vietnam National University, Hanoi.

https://doi.org/10.1016/j.jsamd.2023.100608

along a vortex core was calculated [23–25]. The major quest of vortex states for non-volatile storage applications is the switching of vortex polarity or circularity (i.e. writing) by external perturbations. The first observation of vortex core switching by AC electric current through a vortex state was performed by Van et al. [26,27]. Vortex core switching by rotating magnetic field with inducing spin polarized currents and by frequency dependent perpendicular magnetic fields have also been performed [28,29]. The circularity has been switched using magnetic force microscope (MFM) tips [30], by nanosecond field pulses [31] and by electric fields [32,33]. The chirality determination (i.e. reading) has been done by several electrical techniques like anisotropy magnetoresistance (AMR) [34–36], and planar Hall effect (PHE) [37]. Imaging techniques like MFM [14,38], Magneto-Optic Kerr effect (MOKE), X-ray photoemission electron microscopy (XPEEM) [18], scanning electron microscope with polarization analyzer (SEMPA) [39] and magnetic transmission soft X-ray microscopy (MTXM) [11,31,40,41] have also been employed for circularity and polarity determination.

Vortex states have also been realized in FeGa microstructures fabricated on piezoelectric substrates, enabling voltage-induced control of magnetization via magnetoelastic coupling to the substrate [42,43]. FeGa is a good candidate for microstructures to be used in various applications due to its high magnetostriction, magnetic softness and ductility [44–46]. However, an in-depth investigation of magnetization reversal and possible domain configurations in FeGa microstructures is less performed. In this work, $Fe_{80}Ga_{20}$ and $Fe_{70}Ga_{30}$ disks with different dimensions are fabricated. These compositions possess the peak magnetostriction constants (w.r.t at% Ga) which makes them susceptible to magnetic state changes under external strain. It has been reported that disks with smaller diameter ~300 nm tend to stabilize single domain structures at remanence due to high shape anisotropy [47]. In contrast, disks with larger diameter ~10 μm stabilize multi-domain structures due to larger dipolar coupling [43]. Hence, we have chosen the diameter of the disks in the range of 1–2.8 μm, to generate a balance of shape anisotropy energy and magnetic dipolar energy where possible vortex states can be stabilized. Magnetic domain images were recorded at various applied magnetic field values, revealing the spin textures forming at each stage of the hysteresis curve. Micromagnetic simulations have been performed to understand the experimental results and precisely define the evolution of spin textures during reversal. To achieve implementation of nanostructures in memory applications, a better understanding of vortex formation and control has to be gained. This work shows the stabilization of vortex states through magnetization reversal mechanism in FeGa disks with different sizes and compositions.

2. Experimental

2.1. Fabrication method

FeGa disk arrays were fabricated by means of direct write laser lithography on SiO_2/Si substrates followed by sputtering. The substrates had a thermally oxidized SiO_2 layer with thickness of 500 nm. Focused laser spot was exposed on selected regions of the resist-coated substrate and which was further placed inside a developer and ultrasonification was performed to remove the areas exposed. Circular holes having center-to-center distance of approximately 3 μm were prepared as an array of 33 × 33 elements. The size of the holes depends on the power of the laser used, which decides the final diameter of the disks. Increase in power of laser influences greater reflections from the substrate, resulting in an increase of net exposed area. Further, sputtering was exploited to fill the holes with FeGa alloys. $Fe_{80}Ga_{20}$ and $Fe_{70}Ga_{30}$ targets were used for deposition. $Fe_{70}Ga_{30}$ disks were fabricated using RF sputtering at room temperature. The base pressure of the chamber was 10^{-7} mbar and the deposition pressure was kept at 1.2×10^{-2} mbar. For the preparation of $Fe_{80}Ga_{20}$ disks, triode sputtering was used. The base pressure was 3.9×10^{-6} mbar. The deposition rate was kept at 1.33 Å/s. The resist around the disks, and the metallic deposits on top of it are then removed by acetone washing and subsequent cleaning, leaving the desired disk arrays.

2.2. Structural characterization methods

Scanning electron microscope equipped with an energy dispersive detector (SEM-EDS) was used to observe the morphology of the FeGa disks. In order to verify the composition of FeGa in the disk arrays, additional FeGa thin films were prepared on bare substrates with the same deposition conditions as for the patterned ones. The composition of the films as recorded by EDS was found to be 69.4 %at Fe and 30.6 %at Ga, similar to the $Fe_{70}Ga_{30}$ target. Similar values were observed with the concentration determined by ICP-OES i.e. 69.39 %at Fe and 30.61 %at Ga [46]. Similarly, the composition of a $Fe_{80}Ga_{20}$ thin film were near to 81.3 %at Fe and 18.7 %at Ga, as recorded by EDS.

2.3. Magnetic characterization methods

Magnetization reversal was studied by means of a magneto-optic Kerr effect (MOKE) microscope by Evico magnetics and using an oil immersion lens with a magnification of 100×. The magnetic domains in the disks were recorded at different in-plane magnetic field intensities and the corresponding magnetic hysteresis loops were reconstructed based on the change in image contrast. Magnetic force microscope (MFM) by Bruker Multimode V Nanoscope 8, was used under the application of an in-plane magnetic field (intensity up to 60 mT), to analyze the magnetic configuration (out-of-plane stray magnetic fields) within individual disks with higher spatial resolution. The magnetic tips used in our measurements were MESP-HR10 (resonant frequency of 89 kHz with Co/Cr reflective coating and coercive field of ~ 95 mT). The height of the tip was kept at 101 nm to obtain the best quality images.

2.4. Simulation techniques

Micromagnetic simulations were performed to understand the domain configuration and the magnetic hysteresis of individual FeGa disks using mumax^3 [48]. The geometrical parameters obtained by atomic force microscopy (AFM) were incorporated (Supplementary Fig. S1). The saturation magnetization (M_S) values of the $Fe_{80}Ga_{20}$ and $Fe_{70}Ga_{30}$ alloys were determined to be 1030 kA/m and 820 kA/m, respectively, by measuring the magnetic moment of the continuous thin films using alternating gradient field magnetometer (AGFM). Local variations in magnetic anisotropy were considered using a built-in 2D Voronoi tessellation function. The first order magneto-crystalline anisotropy constant (Kc_1) was considered to be 60 kJ/m^3 with a 10 percent average magnitude variation between the grains. The exchange constant (A) was taken as 14 pJ/m [49]. The damping constant (α) and the cell size were kept at 0.007 and $6 \times 6 \times 6$ nm^3. Periodic boundary conditions were considered with 3 repetitions of disks along x and y directions. The distance between the disks was maintained at 3 μm, matching the experimental design and considering the magnetostatic interactions between the disks. The simulations were performed under an in-plane magnetic field with intensity up to 500 mT.

3. Results and discussion

Fig. 1(a) represents the magnetic hysteresis curve ($M - H$) of $Fe_{80}Ga_{20}$ disk array recorded with application of in-plane magnetic field using longitudinal MOKE. The applied magnetic field was varied in the range of ±20 mT. The loop corresponds to variation in intensity of polarized Kerr signal obtained from a 4 × 4 disk array with a diameter of 2.3 μm and thickness of 24 nm. The saturation field value is recorded to be 12.14 mT. The normalized remanent magnetization recorded is low with a value of 0.11. The loop obtained from a larger disk array is shown in Supplementary Fig. S2, where a smoother and averaged contribution of magnetic contrast is achieved. The opening of the loop, i.e., the vertical distance of the two loop branches at any given applied field, seems increased when saturation is approached. In nanostructures, this behavior is typical to the nucleation of a vortex state below saturation level and its stabilization at remanence. The domain textures in these disks were recorded using a Kerr microscope at different magnetic field intensities as shown in Fig. 1(b)–(g). They correspond to the respective points marked in the hysteresis loop. The single domain state pointing along the +x direction is shown by the dark contrast in the disks, represented in Fig. 1(b). The bright contrast in the disks (Fig. 1(g)) refers to a saturated single domain state aligned along the −x direction. When the field is decreased from 20 mT to 6.1 mT, slight bright contrast is observed at the bottom of the disks which marks the rotation of spins. The bright contrast increases at the remanent state, and forms a spin rotation representing a vortex-like state (Fig. 1(d)). The domain contrast is evidenced as a curling of magnetization in a CW pattern. The simultaneous acquisition of the Kerr contrast for longitudinal and transverse components was obtained for visualization of magnetization orientation as shown in Supplementary Fig. S3. The dark contrast further decreases as the field value is increased in the −x direction (Fig. 1(e)) and almost annihilates as the negative saturation field is approached as observed in Fig. 1(f). The CW rotation of magnetization is observed for a majority of disks during the positive to negative field reversal. However, for some disks of the array (Supplementary Fig. S2), a CCW rotation is also observed. During the negative to positive field cycle, CCW vortex patterns becomes the majority. In both the cycles, the nucleation of vortex core is observed from the bottom of the disks which stabilizes CW and CCW in the first and the second cycle, respectively. An equal probability of CW and CCW vortices was also achieved when an AC field was applied with decreasing magnitude to obtain a demagnetized state (shown in Supplementary Fig. S4). The chirality of the vortex states in magnetic disks can also be affected due to symmetry breaking causing intrinsic Dzyaloshinskii–Moriya interaction (DMI) [11]. However, in our case, the surface related defects and slight shape deformation during the fabrication process are resulting in irregular circularity of vortex [39].

The magnetic configurations of the $Fe_{80}Ga_{20}$ disks were also recorded with MFM due to its ability to detect stray magnetic signals at higher resolution (tens of nm). Fig. 2(a)–(c) represent MFM images of the 3 × 3 disk array with diameter of 2.3 μm which is a portion of the larger array that was recorded with MOKE. The images were recorded by applying a constant in-plane magnetic field and scanning the tip over the sample surface for stray magnetic signals. Fig. 2(a) and (c) represents the single domain states recorded beyond saturation field values of +50 mT and −50 mT, respectively. In Fig. 2(a), the contrast changes from bright to dark (left to right) which indicates a single domain state pointing along the +x direction. Similarly, a single domain state pointing along the −x direction is seen in Fig. 2(c) where the dark to bright (left to right) contrast change is observed. At remanence, a flux closure domain pattern is observed representing a vortex-like magnetic state as shown in Fig. 2(b). The dark lines represent domain walls with a vortex core at the center [33,50]. A different color scale was used to better visualize the vortex core and the domain walls forming during magnetization rotation (Supplementary Fig. S5).

The domain structures were also recorded as a function of field for $Fe_{80}Ga_{20}$ disks with a lower diameter of 1.4 μm, represented by Fig. 2(d)–(f). Single domain states were observed at saturation field values of +50 mT (magnetization along +x direction) and −50 mT (magnetization along −x direction). The domain states recorded at remanence (Fig. 2(e)) are similar to the states observed in Fig. 2(b). Slight perturbations in the intensity of domains were detected during the scanning of the tip. This can be a result of the lower stray field of the domain walls observed for the soft FeGa alloy as compared to hard ferromagnets, as reported in literature [32].

Similar magnetic disks were also fabricated for the $Fe_{70}Ga_{30}$ alloy composition to understand the variation of domain structures forming during magnetization reversal as a function of alloy composition. The diameter and thickness of the disks were nearly 2.2 μm and 24 nm. The magnetic hysteresis curve and the domain structures forming during the reversal, are shown in Fig. 3(a)–(g). The normalized remanent magnetization is recorded to be 0.83 and

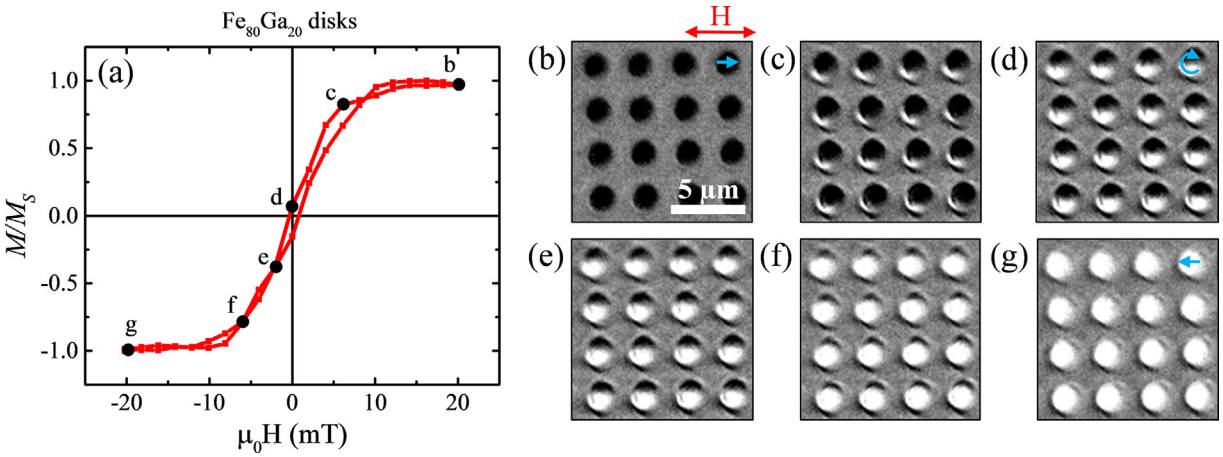

Fig. 1. Magnetic hysteresis curve measured using longitudinal MOKE for a $Fe_{80}Ga_{20}$ disk array of 4 × 4 elements is shown in (a). The diameter and the thickness of the disks are 2.3 μm and 24 nm, respectively. The magnetic domain images are shown in (b)–(g) representing the points marked in the hysteresis loop. The scale bar and the field direction are shown in (b) and are the same for all the domain textures.

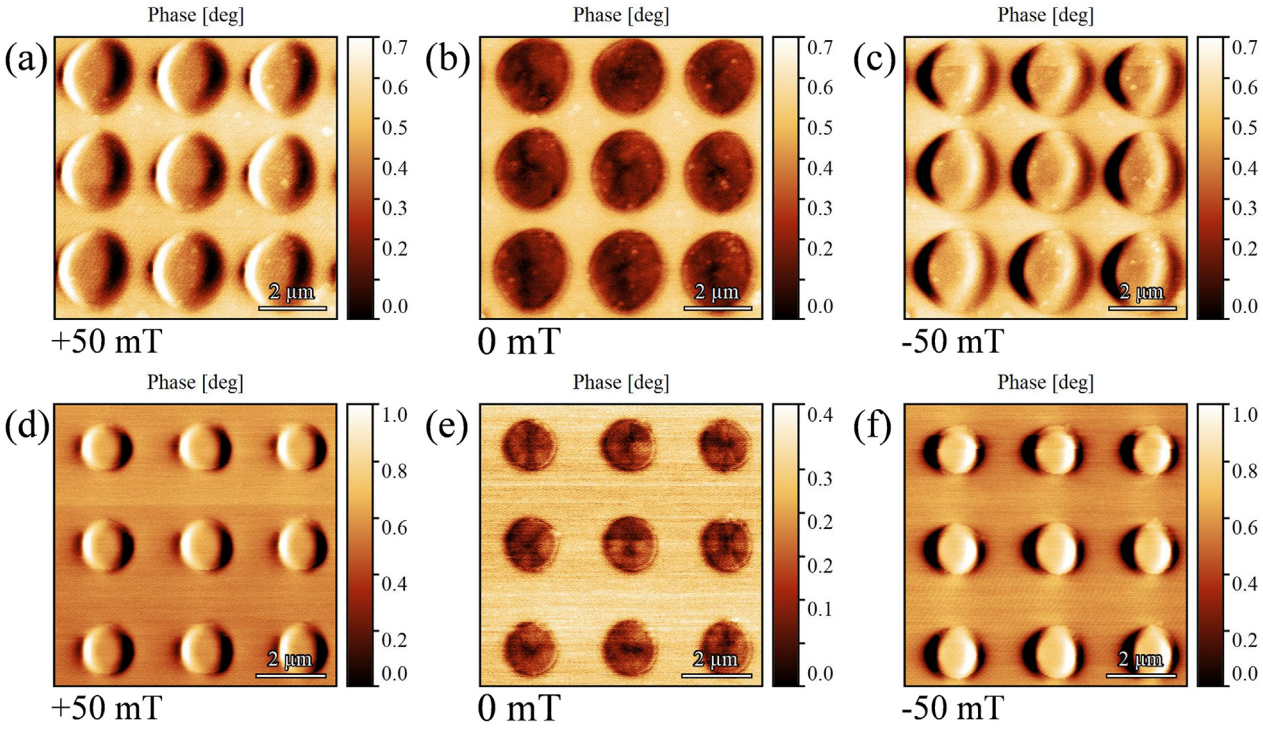

Fig. 2. Magnetic domain textures of the $Fe_{80}Ga_{20}$ disks of diameter 2.3 μm and 1.4 μm measured using MFM. (a), (b) and (c) represents the 2.3 μm disks with in-plane magnetic field of +50 mT (positive saturation), 0 mT (remanence) and −50 mT (negative saturation), respectively. (d), (e) and (f) represents the 1.4 μm disks at +50 mT, 0 mT and −50 mT, respectively.

a coercive field to be 6.1 mT. The saturation field value is measured to be 26.1 mT. Fig. 3(b)–(g) represent the domain images as marked to the respective field intensities in the hysteresis curve. The single domain states at negative saturation field is represented by the disks with bright contrast as shown in Fig. 3(b). Near remanence, slight dark contrast is observed at disk edges due to the rotation of spins (Fig. 3(c)). With further increase in field, near 4.6 mT, a bright-dark-bright contrast is observed in some of the disks as marked by the yellow circles in Fig. 3(d). The longitudinal and transverse magnetization components were acquired simultaneously to understand the possible domain configuration (Supplementary Fig. S3). The bright-dark contrast at the top suggest a CCW rotation of magnetization and the dark-white suggest a CW rotation. These states may symbolize the stabilization of a double vortex state as also reported in literature for Permalloy [51]. The dark contrast increases and appears in all the disks as the field is increased to 7.6 mT and small bright contrasts are only left at the top and bottom portions in some disks (Fig. 3(e)). It can also be observed that there is a single vortex nucleation in some of the disks (green circles), which can be attributed to the shape deformity and uneven sizes of the disks. As the positive saturation field is approached, the spins align along the +x direction with very minimal bright contrast in Fig. 3(f). A completely positive saturated state is observed in Fig. 3(g).

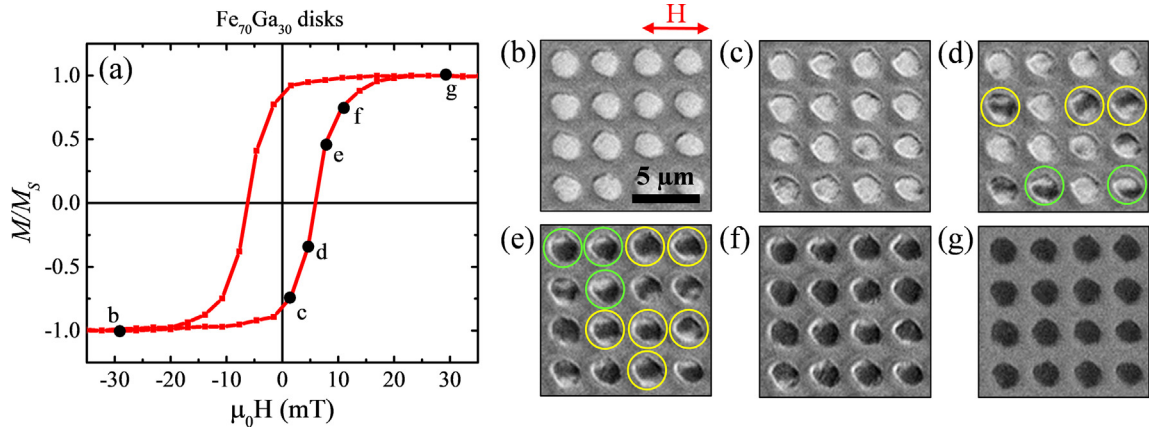

Fig. 3. Magnetic hysteresis curve measured using longitudinal MOKE for a $Fe_{70}Ga_{30}$ disk array of 4 × 4 elements is shown in (a). The diameter and the thickness of the disks are 2.2 μm and 24 nm, respectively. The magnetic domain images are shown in (b)–(g) representing the points marked in the hysteresis loop. The yellow and green circles represent the disks stabilizing a double vortex and single vortex state, respectively. The scale bar and the field direction are shown in (b) and are the same for all the domain textures.

The domain states in the $Fe_{70}Ga_{30}$ disks having a diameter of 1.8 μm and a thickness of 18 nm were recorded with MFM. A 2 × 2 array was chosen from the larger array of 33 × 33 array. At a field value of +60 mT (positive saturation), single domain states with bright-dark contrast (left-right) pointing along the +x direction are observed (Fig. 4(a)). Similarly, domains pointing along the −x direction are observed at −60 mT with opposite contrast (dark-bright) as observed in Fig. 4(c). At the positive remanent state, shown in Fig. 4(b), a multidomain state is observed. The central bright region is surrounded by darker regions (having antiparallel configurations) which can resemble to the stabilization of a double vortex state. Similar states observed under MFM in 1 μm diameter Co disks were reported previously by Prejbeanu et al. [20].

The magnetic hysteresis curves were extracted from MOKE measurements for two separate $Fe_{70}Ga_{30}$ disks individually from a larger array (shown in Supplementary Fig. S7) where a vortex state and a double vortex state were observed during reversal, as shown in Fig. 5(a) and (b), respectively. The evolution of magnetic domain in the disks is observed along both the branches of the hysteresis curve. In disk 1, dark contrast is observed at the bottom of the disk as the coercive field is approached (Fig. 5(a)2) which mark the nucleation of a vortex state. The dark contrast increases in Fig. 5(a) 2−5(a)5 gradually, indicating the rotation of magnetic moments along +x direction and the vortex core moving up. On the other side of the branch (Fig. 5(a)7−5(a)10), bright contrast is observed to be formed in a similar pattern representing a vortex with opposite circularity as compared to the vortex formed in the first branch. For

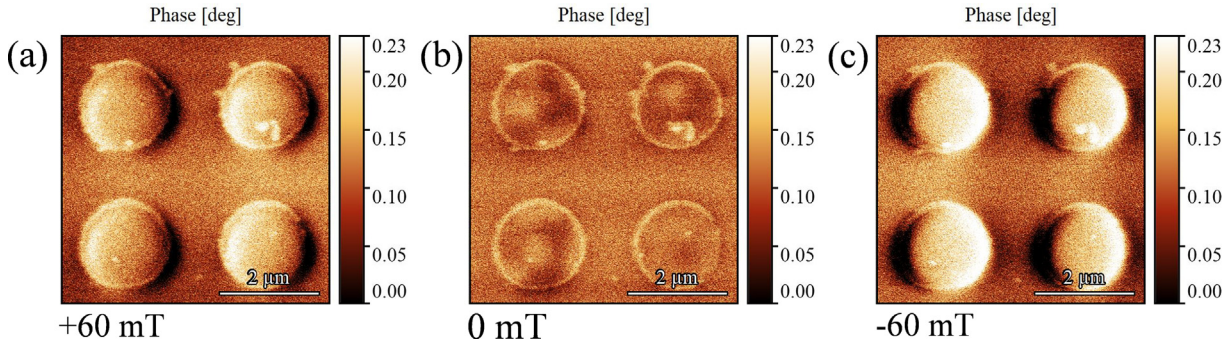

Fig. 4. Magnetic domain textures of $Fe_{70}Ga_{30}$ disks with diameter of 1.8 μm with in-plane applied field of +60 mT (positive saturation), 0 mT (remanence) and −60 mT (negative saturation) is shown by (a), (b) and (c), respectively.

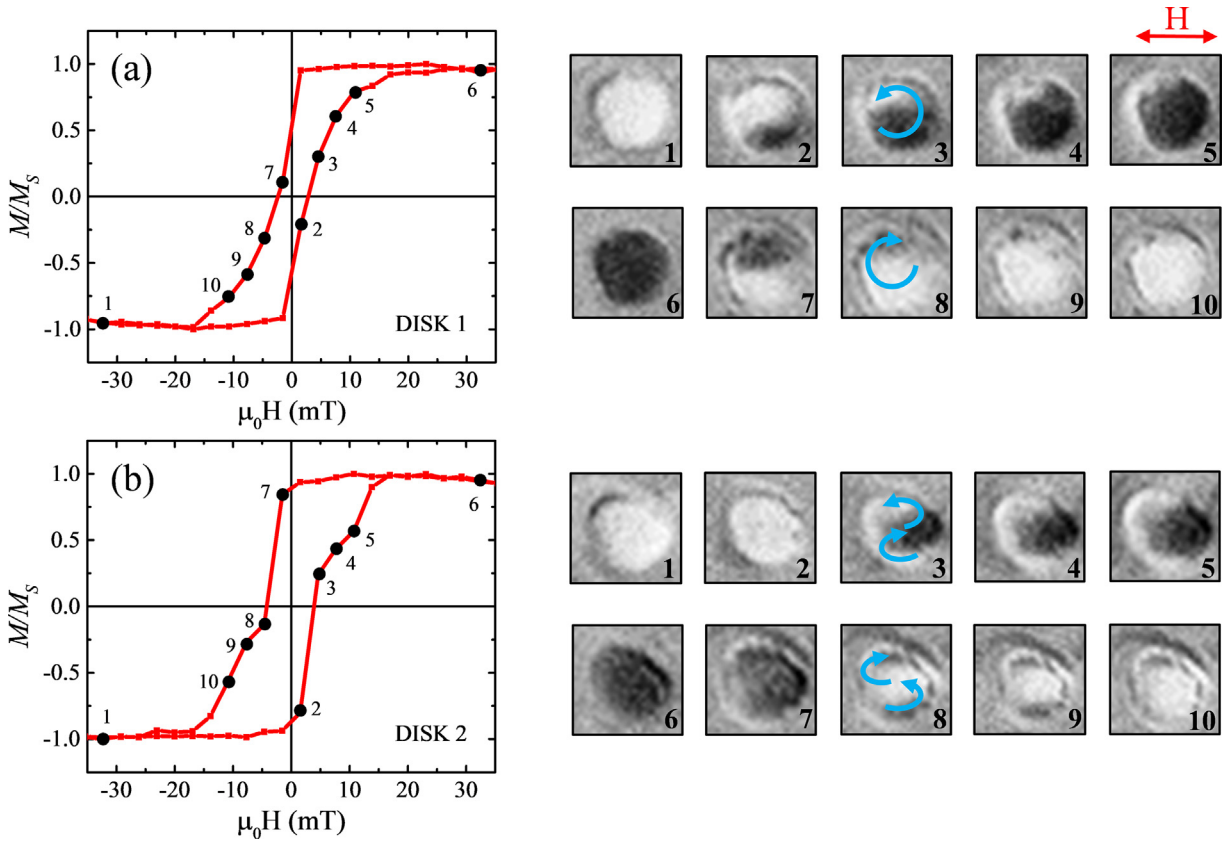

Fig. 5. (a) and (b) represent the magnetic hysteresis curve of two individual disks chosen from a larger array of $Fe_{70}Ga_{30}$ disks with diameter of 2.3 μm. (a)1−(a)10 and (b)1−(b)10 represent the domain structures formed in disk 1 and disk 2, respectively, during magnetization reversal as marked in the corresponding hysteresis curves.

disk 2, as shown in Fig. 5(b)3–5(b)5, the formation of a double vortex state is evident from the bright-dark-bright contrast. A change in the slope of the hysteresis is marked after the formation of a double vortex state. This is due to the requirement of more Zeeman energy to annihilate the stable structure and reach to a saturated state. Similar state is also recorded on the other branch of the hysteresis where is dark-bright-dark pattern is observed in Fig. 5(b)8–5(b)10.

In order to understand the exact spin textures of the domain states observed experimentally, micromagnetic simulations were performed using the optimal material parameters. Fig. 6(a) shows the simulated magnetic hysteresis curve of a circular $Fe_{70}Ga_{30}$ disk with a diameter of 1.4 μm and thickness of 24 nm. The observed hysteresis behavior corresponds to nucleation and stabilization of a vortex-type state similar to the behavior observed experimentally in Fig. 5(a). The spin configuration of the disk near the coercive field is shown in Fig. 6(b) where a typical vortex state is observed. The color wheel represents the direction of the magnetic moments, where red and sky blue points along +x and −x directions, respectively. The x-component of the magnetization is shown with black and white scale(+x and −x) in Fig. 6(c) where the contrast is similar to the state observed experimentally in MOKE (Fig. 6(d)). The circularity of the vortex state is CCW. The vortex core moves up and annihilates at the top of the disk at saturation as more magnetic moments start curling along the +x direction. The inhomogeneity in the contrast of the disks is due to the dispersion of anisotropy and the grain sizes across the simulated area. The variation in anisotropy and grain distribution is represented by Fig. 6(e) with an enlarged view. Fig. 6(f) demonstrates the simulated hysteresis of another $Fe_{70}Ga_{30}$ disk with same thickness and a higher diameter of 1.8 μm. The domain configuration near coercivity is a double vortex state as represented in Fig. 6(g). The x-component of the state shown in Fig. 6(h), is similar to the bright-dark-bright state as observed in MOKE. The comparison of Fig. 6(a) and (f) shows that the hysteresis of a disk stabilizing a double vortex state is more squared with higher coercive field than that of a single vortex state. This characteristic of disks stabilizing different states are also observed experimentally, as shown in Fig. 5(a) and (b). The plots of micromagnetic energies as a function of field, that are considered in the simulations are shown in Supplementary Fig. S9.

The magnetization reversal and domain structures were simulated for different diameters and thicknesses of the disk to determine the possible stable states. This was performed to overcome the experimental limitations and constraints for such wide range of parameters. A 2D plot of magnetization configurations forming during the magnetic reversal for the $Fe_{80}Ga_{20}$ and $Fe_{70}Ga_{30}$ disks are shown in Fig. 7(a) and (b), respectively. The formation of S-domain states (red squares) are limited to 18 nm thickness of the $Fe_{80}Ga_{20}$ disks whereas the range expands to 30 nm in the $Fe_{70}Ga_{30}$ ones. In the S-domain state, the moments in the central part of the disk start curling along the direction of applied field forming a S-shaped spin configuration. Single vortex states (yellow circles) are observed for lower diameters of the disks due to less dipolar energies. The range of diameters, where a single vortex state can be stabilized in higher for the $Fe_{70}Ga_{30}$ disks. For relatively higher diameters and thickness of the disks, double vortex states (blue

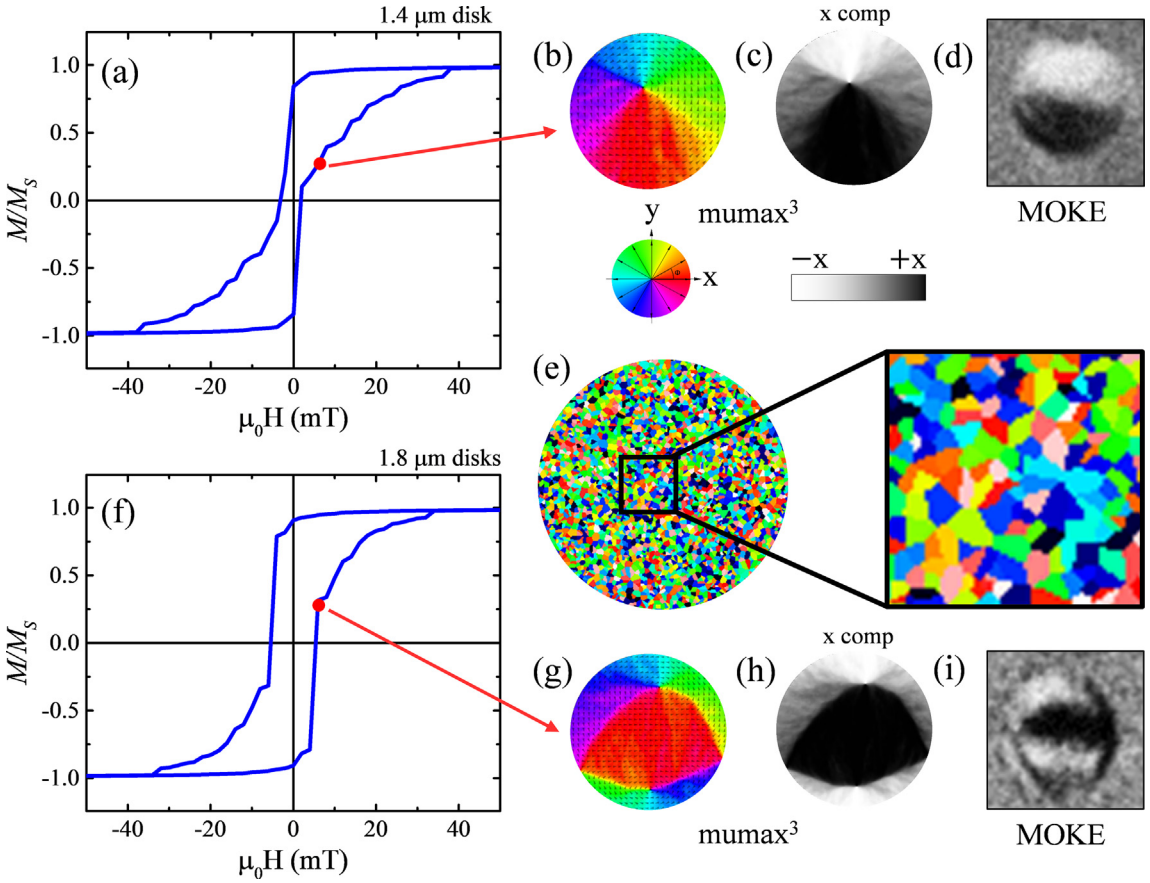

Fig. 6. Simulated magnetic hysteresis curves of $Fe_{70}Ga_{30}$ disks with diameter of 1.4 μm and 1.8 μm are shown in (a) and (f), respectively. In the 1.4 μm disk, single vortex state is observed near coercive field, represented by (b). The corresponding x-component of the magnetization (c) looks similar to the experimental observed state (d). In the 1.8 μm disk, double vortex state is observed near coercive field (g). The corresponding x-component of the magnetization (h) looks similar to (i). The distribution of grains having an anisotropy, shape and size variation is shown by (e).

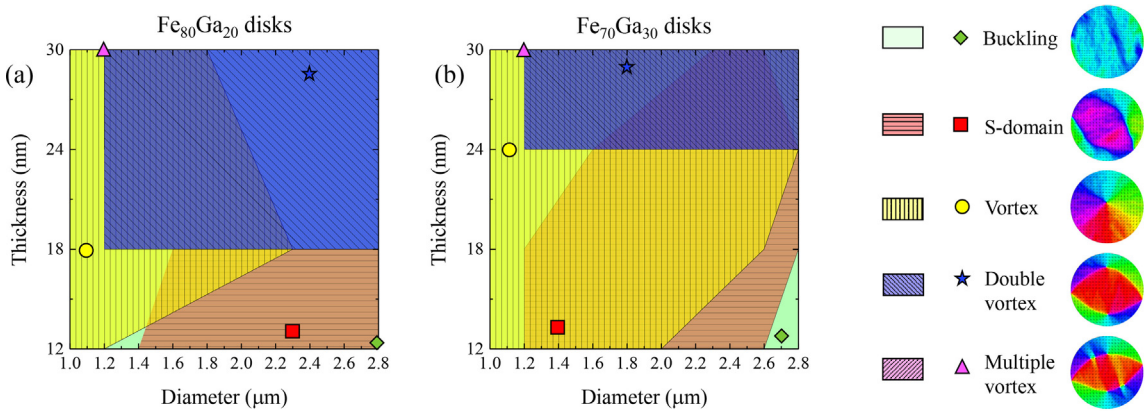

Fig. 7. Phase diagrams representing the different domain configurations forming during magnetization reversal in disks of different thicknesses and diameters. (a) and (b) correspond to the $Fe_{80}Ga_{20}$ and $Fe_{70}Ga_{30}$ compositions, respectively. The buckling, S-domain, vortex, double vortex and multiple vortex states are represented by green diamonds, red squares, yellow circles, blue stars and pink triangles, respectively. The physical representations of the spin configurations are shown on the right.

stars) are observed. Multiple vortex which are meta-stable states (pink triangle) are also observed for higher thickness of 30 nm for most range of the diameter in $Fe_{80}Ga_{20}$ disks. The actual representations of the simulated states obtained here are shown in Supplementary Fig. S10. The buckling states (green diamonds) are observed in every dimension where the magnetization starts to reverse. In a comparison of magnetic state of $Fe_{80}Ga_{20}$ and $Fe_{70}Ga_{30}$ disks with same dimensions, it can be observed that complex spin textures are preferentially more stable in the $Fe_{80}Ga_{20}$ ones. This is due to higher M_S value which tends to generate more demagnetizing energy. The points marked on the phase diagrams represent the lowest energy state during magnetization reversal at the particular dimension. The magnetic states forming during the reversal are dependent on the thickness, the diameter and the composition of the FeGa disks. Hence, the shape anisotropy and the saturation magnetization play a major role in the formation of flux closure domain structures like single vortex or double vortex states.

4. Conclusion

The magnetic domains formed during the magnetization reversal process in FeGa microdisks have been investigated. The change in composition, thickness and diameter of FeGa disks has a significant impact on the reversal process, thereby affecting the hysteresis loop and the domain structures. In the $Fe_{70}Ga_{30}$ disks with diameters ranging between 1.4 and 2.3 μm, single vortex and double vortex states are observed to be stable at room temperature as confirmed with MOKE microscopy and MFM. Single vortex states could only be observed in the $Fe_{80}Ga_{20}$ disks. The comparison of the magnetic hysteresis loops stabilizing a vortex state and a double vortex one showed that the latter has more squareness and high coercivity. The spin arrangements of the experimentally observed domain states were studied using micromagnetic simulations. The simulations confirmed the formation of a vortex, double vortex, multiple vortex states and even S-shaped domains in the $Fe_{80}Ga_{20}$ and $Fe_{70}Ga_{30}$ disks. Our work reveals the magnetic domain structures that can be stabilized in FeGa disks at the micron-scale. These studies can be exploited in the field of data storage applications where the integration of this alloy in memory devices is unexplored.

Declaration of competing interest

The authors declare that they have no known competing financial interests or personal relationships that could have appeared to influence the work reported in this paper.

Acknowledgments

This work has received funding from the European Union's Horizon 2020 research and innovation programme under the Marie Skłodowska-Curie grant agreement No 861145. The experimental work has been partially performed at NanoFacility Piemonte, an INRIM laboratory supported by Compagnia di San Paolo. Czech-NanoLab project LM2018110 funded by MEYS CR is gratefully acknowledged for the financial support of the measurements at CEITEC Nano Research Infrastructure. The authors also thank Adriano Di Pietro for technical help in simulations.

Appendix A. Supplementary data

Supplementary data to this article can be found online at https://doi.org/10.1016/j.jsamd.2023.100608.

References

[1] J.M. Kosterlitz, D.J. Thouless, Ordering, metastability and phase transitions in two-dimensional systems, J. Phys. C Solid State Phys. 6 (7) (1973) 1181.
[2] A. Bogdanov, A. Hubert, Thermodynamically stable magnetic vortex states in magnetic crystals, J. Magn. Magn. Mater. 138 (3) (1994) 255–269.
[3] K.Y. Guslienko, V. Novosad, Y. Otani, H. Shima, K. Fukamichi, Field evolution of magnetic vortex state in ferromagnetic disks, Appl. Phys. Lett. 78 (24) (2001) 3848–3850.
[4] V. Novosad, F.Y. Fradin, P.E. Roy, K.S. Buchanan, K.Y. Guslienko, S.D. Bader, Magnetic vortex resonance in patterned ferromagnetic dots, Phys. Rev. B 72 (2) (2005) 024455.
[5] V. Pribiag, I. Krivorotov, G. Fuchs, P. Braganca, O. Ozatay, J. Sankey, D. Ralph, R. Buhrman, Magnetic vortex oscillator driven by dc spin-polarized current, Nat. Phys. 3 (7) (2007) 498–503.
[6] S. Bohlens, B. Krüger, A. Drews, M. Bolte, G. Meier, D. Pfannkuche, Current controlled random-access memory based on magnetic vortex handedness, Appl. Phys. Lett. 93 (14) (2008) 142508.
[7] T. Kimura, Y. Otani, H. Masaki, T. Ishida, R. Antos, J. Shibata, Vortex motion in chirality-controlled pair of magnetic disks, Appl. Phys. Lett. 90 (13) (2007) 132501.
[8] J.L. Hockel, A. Bur, T. Wu, K.P. Wetzlar, G.P. Carman, Electric field induced magnetization rotation in patterned ni ring/pb (mg1/3nb2/3) o3](1-0.32)-[pbtio3] 0.32 heterostructures, Appl. Phys. Lett. 100 (2) (2012) 022401.
[9] V. Novosad, M. Grimsditch, J. Darrouzet, J. Pearson, S. Bader, V. Metlushko, K. Guslienko, Y. Otani, H. Shima, K. Fukamichi, Shape effect on magnetization reversal in chains of interacting ferromagnetic elements, Appl. Phys. Lett. 82 (21) (2003) 3716–3718.
[10] R.P. Cowburn, D. Koltsov, A. Adeyeye, M. Welland, D. Tricker, Single-domain circular nanomagnets, Phys. Rev. Lett. 83 (5) (1999) 1042.
[11] M.-Y. Im, P. Fischer, K. Yamada, T. Sato, S. Kasai, Y. Nakatani, T. Ono, Symmetry breaking in the formation of magnetic vortex states in a permalloy nanodisk, Nat. Commun. 3 (1) (2012) 1–6.
[12] K.S. Buchanan, P.E. Roy, M. Grimsditch, F.Y. Fradin, K.Y. Guslienko, S.D. Bader, V. Novosad, Soliton-pair dynamics in patterned ferromagnetic ellipses, Nat. Phys. 1 (3) (2005) 172–176.

[13] A. Hubert, R. Schäfer, Magnetic Domains: The Analysis of Magnetic Microstructures, Springer Science & Business Media, 2008.
[14] M. Coïsson, G. Barrera, F. Celegato, A. Manzin, F. Vinai, P. Tiberto, Magnetic vortex chirality determination via local hysteresis loops measurements with magnetic force microscopy, Sci. Rep. 6 (1) (2016) 1–9.
[15] R. Lo Conte, Z. Xiao, C. Chen, C.V. Stan, J. Gorchon, A. El-Ghazaly, M.E. Nowakowski, H. Sohn, A. Pattabi, A. Scholl, et al., Influence of nonuniform micron-scale strain distributions on the electrical reorientation of magnetic microstructures in a composite multiferroic heterostructure, Nano Lett. 18 (3) (2018) 1952–1961.
[16] T. Shinjo, T. Okuno, R. Hassdorf, K. Shigeto, T. Ono, Magnetic vortex core observation in circular dots of permalloy, Science 289 (5481) (2000) 930–932.
[17] X. Zhu, P. Grütter, V. Metlushko, B. Ilic, Magnetization reversal and configurational anisotropy of dense permalloy dot arrays, Appl. Phys. Lett. 80 (25) (2002) 4789–4791.
[18] K. Buchanan, K.Y. Guslienko, A. Doran, A. Scholl, S. Bader, V. Novosad, Magnetic remanent states and magnetization reversal in patterned trilayer nanodots, Phys. Rev. B 72 (13) (2005) 134415.
[19] M. Natali, I. Prejbeanu, A. Lebib, L. Buda, K. Ounadjela, Y. Chen, Correlated magnetic vortex chains in mesoscopic cobalt dot arrays, Phys. Rev. Lett. 88 (15) (2002) 157203.
[20] I. Prejbeanu, M. Natali, L. Buda, U. Ebels, A. Lebib, Y. Chen, K. Ounadjela, In-plane reversal mechanisms in circular co dots, J. Appl. Phys. 91 (10) (2002) 7343–7345.
[21] Z. Dai, Y. Dai, W. Liu, T. Wang, X. Zhao, X. Zhao, Z. Zhang, Magnetization reversal of vortex states driven by out-of-plane field in the nanocomposite co/pd/ru/py disks, Appl. Phys. Lett. 111 (2) (2017) 022404.
[22] P. Tiberto, F. Celegato, G. Barrera, M. Coisson, F. Vinai, P. Rizzi, Magnetization reversal and microstructure in polycrystalline Fe50Pd50 dot arrays by self-assembling of polystyrene nanospheres, Sci. Technol. Adv. Mater. 17 (1) (2016) 462–472.
[23] A. Wachowiak, J. Wiebe, M. Bode, O. Pietzsch, M. Morgenstern, R. Wiesendanger, Direct observation of internal spin structure of magnetic vortex cores, Science 298 (5593) (2002) 577–580.
[24] J. Miltat, A. Thiaville, Vortex cores—smaller than small, Science 298 (5593) (2002), 555–555.
[25] S.-B. Choe, Y. Acremann, A. Scholl, A. Bauer, A. Doran, J. Sto hr, H.A. Padmore, Vortex core-driven magnetization dynamics, Science 304 (5669) (2004) 420–422.
[26] B. Van Waeyenberge, A. Puzic, H. Stoll, K. Chou, T. Tyliszczak, R. Hertel, M. Fähnle, H. Brückl, K. Rott, G. Reiss, et al., Magnetic vortex core reversal by excitation with short bursts of an alternating field, Nature 444 (7118) (2006) 461–464.
[27] K. Yamada, S. Kasai, Y. Nakatani, K. Kobayashi, H. Kohno, A. Thiaville, T. Ono, Electrical switching of the vortex core in a magnetic disk, Nat. Mater. 6 (4) (2007) 270–273.
[28] S.-K. Kim, K.-S. Lee, Y.-S. Yu, Y.-S. Choi, Reliable low-power control of ultrafast vortex-core switching with the selectivity in an array of vortex states by in-plane circular-rotational magnetic fields and spin-polarized currents, Appl. Phys. Lett. 92 (2) (2008) 022509.
[29] B. Pigeau, G. De Loubens, O. Klein, A. Riegler, F. Lochner, G. Schmidt, L. Molenkamp, V. Tiberkevich, A. Slavin, A frequency-controlled magnetic vortex memory, Appl. Phys. Lett. 96 (13) (2010) 132506.
[30] V. Mironov, B. Gribkov, A. Fraerman, S. Gusev, S. Vdovichev, I. Karetnikova, I. Nefedov, I. Shereshevsky, MFM probe control of magnetic vortex chirality in elliptical co nanoparticles, J. Magn. Magn. Mater. 312 (1) (2007) 153–157.
[31] V. Uhlíř, M. Urbánek, L. Hladík, J. Spousta, M. Im, P. Fischer, N. Eibagi, J. Kan, E. Fullerton, T. Šikola, Dynamic switching of the spin circulation in tapered magnetic nanodisks, Nat. Nanotechnol. 8 (5) (2013) 341–346.
[32] Q. Li, A. Tan, A. Scholl, A. Young, M. Yang, C. Hwang, A. N'Diaye, E. Arenholz, J. Li, Z. Qiu, Electrical switching of the magnetic vortex circulation in artificial multiferroic structure of Co/Cu/PMN-PT (011), Appl. Phys. Lett. 110 (26) (2017) 262405.
[33] Y. Zhang, C. Wang, H. Huang, J. Lu, R. Liang, J. Liu, R. Peng, Q. Zhang, Q. Zhang, J. Wang, et al., Deterministic reversal of single magnetic vortex circulation by an electric field, Sci. Bull. 65 (15) (2020) 1260–1267.
[34] P. Vavassori, M. Grimsditch, V. Metlushko, N. Zaluzec, B. Ilic, Magnetoresistance of single magnetic vortices, Appl. Phys. Lett. 86 (7) (2005) 072507.
[35] M. Goto, H. Hata, A. Yamaguchi, Y. Nakatani, T. Yamaoka, Y. Nozaki, Electrical detection of vortex states in a ferromagnetic disk using the rectifying effect, J. Appl. Phys. 109 (7) (2011) 07D306.
[36] M. Sushruth, J.P. Fried, A. Anane, S. Xavier, C. Deranlot, M. Kostylev, V. Cros, P.J. Metaxas, Electrical measurement of magnetic-field-impeded polarity switching of a ferromagnetic vortex core, Phys. Rev. B 94 (10) (2016) 100402.
[37] Y. Huang, C. Wang, A. Adeyeye, Determination of vortex chirality using planar hall effect, J. Appl. Phys. 100 (1) (2006) 013909.
[38] M. Coïsson, G. Barrera, F. Celegato, E. Enrico, A. Manzin, E.S. Olivetti, P. Tiberto, F. Vinai, Local field loop measurements by magnetic force microscopy, J. Phys. D Appl. Phys. 47 (32) (2014) 325003.
[39] M. Konoto, T. Yamada, K. Koike, H. Akoh, T. Arima, Y. Tokura, Formation and control of magnetic vortex chirality in patterned micromagnet arrays, J. Appl. Phys. 103 (2) (2008) 023904.
[40] A. Vansteenkiste, K. Chou, M. Weigand, M. Curcic, V. Sackmann, H. Stoll, T. Tyliszczak, G. Woltersdorf, C. Back, G. Schütz, et al., X-ray imaging of the dynamic magnetic vortex core deformation, Nat. Phys. 5 (5) (2009) 332–334.
[41] P. Fischer, M.-Y. Im, S. Kasai, K. Yamada, T. Ono, A. Thiaville, X-ray imaging of vortex cores in confined magnetic structures, Phys. Rev. B 83 (21) (2011) 212402.
[42] D. Parkes, R. Beardsley, S. Bowe, I. Isakov, P. Warburton, K. Edmonds, R. Campion, B. Gallagher, A. Rushforth, S. Cavill, Voltage controlled modification of flux closure domains in planar magnetic structures for microwave applications, Appl. Phys. Lett. 105 (6) (2014) 062405.
[43] M.G. De Jesus, Z. Xiao, M. Goiriena-Goikoetxea, R.V. Chopdekar, M.K. Panduranga, P. Shirazi, A. Acosta, J.P. Chang, J. Bokor, G.P. Carman, et al., Magnetic state switching in FeGa microstructures, Smart Mater. Struct. 31 (3) (2022) 035005.
[44] A.E. Clark, J.B. Restorff, M. Wun-Fogle, T.A. Lograsso, D.L. Schlagel, Magnetostrictive properties of body-centered cubic Fe-Ga and Fe-Ga-al alloys, IEEE Trans. Magn. 36 (5) (2000) 3238–3240.
[45] J. Atulasimha, A.B. Flatau, A review of magnetostrictive iron—gallium alloys, Smart Mater. Struct. 20 (4) (2011) 043001.
[46] G. Pradhan, F. Celegato, G. Barrera, E.S. Olivetti, M. Coisson, J. Hajduček, J.A. Arregi, L. Čelko, V. Uhlíř, P. Rizzi, et al., Magnetic properties of FeGa/kapton for flexible electronics, Sci. Rep. 12 (1) (2022) 1–11.
[47] H. Ahmad, J. Atulasimha, S. Bandyopadhyay, Reversible strain-induced magnetization switching in FeGa nanomagnets: pathway to a rewritable, non-volatile, non-toggle, extremely low energy straintronic memory, Sci. Rep. 5 (1) (2015) 1–7.
[48] A. Vansteenkiste, J. Leliaert, M. Dvornik, M. Helsen, F. Garcia-Sanchez, B. Van Waeyenberge, The design and verification of MuMax3, AIP Adv. 4 (10) (2014) 107133.
[49] T. Brintlinger, S.-H. Lim, K.H. Baloch, P. Alexander, Y. Qi, J. Barry, J. Melngailis, L. Salamanca-Riba, I. Takeuchi, J. Cumings, In situ observation of reversible nanomagnetic switching induced by electric fields, Nano Lett. 10 (4) (2010) 1219–1223.
[50] J. Garcıa, A. Thiaville, J. Miltat, K. Kirk, J. Chapman, F. Alouges, Quantitative interpretation of magnetic force microscopy images from soft patterned elements, Appl. Phys. Lett. 79 (5) (2001) 656–658.
[51] B. Hong, T. Hayward, C. Barnes, J.-R. Jeong, Double vortex interaction in micron-sized elliptical ni _{80} fe _{20} elements studied by real-time kerr microscopy, IEEE Trans. Magn. 45 (6) (2009) 2511–2514.